SIMULATION OF FLAME ACCELERATION AND DDT IN H_2-AIR MIXTURE WITH A FLUX LIMITER CENTRED METHOD

Vaagsaether, K.[1], Knudsen, V.[1] and Bjerketvedt, D.[1]
[1]Department of Technology, Telemark University College, Kjolnes Ring 56, Porsgrunn, NO-3918, Norway

ABSTRACT

Flame acceleration and deflagration to detonation transition (DDT) is simulated with a numerical code based on a flux limiter centered method for hyperbolic differential equations [1]. The energy source term is calculated by a Riemann solver for the inhomogeneous Euler equations for the turbulent combustion and a two-step reaction model for hydrogen-air. The transport equations are filtered for large eddy simulation (LES) and the sub-filter turbulence is modelled by a transport equation for the the turbulent kinetic energy [2]. The flame tracking is handled by the G-equation for turbulent flames [3]. Numerical results are compared to pressure histories from physical experiments. These experiments are performed in a closed, circular, 4 m long tube with inner diameter of 0.107 m. The tube is filled with hydrogen-air mixture at 1 atm, which is at rest when ignited. The ignition is located at one end of the tube. The tube is fitted with an obstruction with circular opening 1 m down the tube from the ignition point. The obstruction has a blockage ratio of 0.92 and a thickness of 0.01 m. The obstruction creates high pressures in the ignition end of the tube and very high gas velocities in and behind the obstruction opening. The flame experiences a detonation to deflagration transition (DDT) in the supersonic jet created by the obstruction. Pressure build-up in the ignition end of the tube is simulated with some discrepancies. The DDT in the supersonic jet is simulated, but the position of the DDT is strongly dependent on the simulated pressure in the ignition end.

NOMENCLATURE

C_S	Smagorinsky constant
C_ε	destruction of turbulence constant
E	energy per volume
F	flux of conserved variables
k	turbulent kinetic energy
p	pressure
q	heat released per mass
r	slope strength
S	strain rate tensor
t	time variable
T	temperature
u	velocity component
u	velocity vector
U	conserved variable
v_f	particle velocity in front of flame
x	spatial variable
z	reaction variable
α	radical reaction variable
Δ	filter length scale
ϕ	flux limiter
ν_t	turbulent kinematic viscosity
ρ	density
σ_t	turbulent Prandtl number
τ	turbulent shear stress

1.0 INTRODUCTION

A numerical code for 1D, 2D and 3D simulations of combustion processes, including detonations and deflagration to detonation transition (DDT), is proposed. The code is based on a 2nd order accurate total variation diminishing (TVD), flux limiter centered scheme. The goal of this project is to create a code that can simulate the propagation of a combustion wave from a weak ignition to detonation. Since the detonation wave is a shock wave, and the flame creates shock waves, a TVD method must be used as the numerical scheme. The TVD scheme ensures capturing of discontinuities in the solution. A 2nd order centered scheme is chosen because of its simplicity and computational speed, but it may smoothen shocks over more computational cells than a upwind scheme. Vaagsaether and Bjerketvedt have tested the ability of the scheme to simulate turbulence in compressible, supersonic flow [4]. Numerical experiments are compared with physical experiments by Knudsen et.al. [5] that are executed in a 4 m long circular tube that is closed in both ends. The tube is fitted with an obstruction to create turbulence and high gas velocities. The codes ability to simulate non-reactive flow have been validated against theoretical and physical experiments, as well. These tests will not be presented in this paper.

2.0 NUMERICAL SCHEME AND MODELS

The codes solution process is first to solve the hyperbolic part of the differential equations in one direction with the FLIC scheme. Then the other terms of the equations are solved with the time dependent term. The numerical scheme is explained in detail in chapter 2.1. The turbulence model is explained in chapter 2.2 and the combustion models are explained in chapter 2.3.

2.1 Numerical Scheme

TVD schemes for convective transport are constructed for hyperbolic PDEs, such as the Euler equations shown in equations 1 and 2. The equations are discretised on a LES grid, and are filtered with a box filter or top-hat filter in physical space. The numerical scheme is created for one space dimension.

$$\frac{\partial \boldsymbol{U}}{\partial t}+\frac{\partial \boldsymbol{F}(\boldsymbol{U})}{\partial x}=0 \tag{1}$$

$$\boldsymbol{U}=\begin{bmatrix}\bar{\rho}\\ \bar{\rho}\tilde{u}\\ \tilde{E}\end{bmatrix} \qquad \boldsymbol{F}=\begin{bmatrix}\bar{\rho}\tilde{u}\\ \bar{\rho}\tilde{u}^2+\tilde{p}\\ \tilde{u}(\tilde{E}+\tilde{p})\end{bmatrix} \tag{2}$$

The FLIC scheme is a 2nd order accurate centred flux-limiter scheme that combines the 1st order accurate FORCE scheme and the 2nd order Richtmyer version of the Lax-Wendroff scheme. The FORCE flux is a deterministic version of the Random Choice Method, where the stochastic steps of the RCM is replaced by integral averages of the Riemann problem solutions. One outcome of this is that the FORCE flux is the arithmetic mean of the Richtmyer flux and the Lax-Friedrich flux. The 1st order Lax-Friedrich flux is defined in equation 3.

$$\boldsymbol{F}^{LF}_{i+\frac{1}{2}}=\frac{1}{2}\left[\boldsymbol{F}(\boldsymbol{U}_L)+\boldsymbol{F}(\boldsymbol{U}_R)\right]+\frac{1}{2}\frac{\delta x}{\delta t}\left[\boldsymbol{U}_L-\boldsymbol{U}_R\right] \tag{3}$$

Subscript L and R denotes the the left and right cell of an inter cell boundary. The 2nd order Richtmyer flux is defined by the intermediate states of the conserved variables as shown in equation 4.

$$\boldsymbol{U}^{RI}_{i+\frac{1}{2}}=\frac{1}{2}\left[\boldsymbol{U}_L+\boldsymbol{U}_R\right]+\frac{1}{2}\frac{\delta t}{\delta x}\left[\boldsymbol{F}(\boldsymbol{U}_L)-\boldsymbol{F}(\boldsymbol{U}_R)\right] \tag{4}$$

$$\boldsymbol{F}^{RI}_{i+\frac{1}{2}}=\boldsymbol{F}(\boldsymbol{U}^{RI}_{i+\frac{1}{2}}) \tag{5}$$

And the FORCE flux

$$\boldsymbol{F}^{\boldsymbol{FORCE}}_{\boldsymbol{i+\frac{1}{2}}} = \frac{1}{2}\left[\boldsymbol{F}^{\boldsymbol{LF}}_{\boldsymbol{i+\frac{1}{2}}} + \boldsymbol{F}^{\boldsymbol{RI}}_{\boldsymbol{i+\frac{1}{2}}}\right] \tag{6}$$

The flux limiters control the order of the scheme. For areas where the solution is smooth, the scheme is 2nd order accurate or close to 2nd order. For areas with discontinuous solutions the scheme is 1st order accurate. A measure of the smoothness of the solution is needed to construct the flux limiter. Since the total energy includes all wave families, it is a good choice for the defining variable of the flux limiter. The slope r is defined for the left and right inter cell boundary

$$r^{L}_{i+\frac{1}{2}} = \frac{\delta E_{i-\frac{1}{2}}}{\delta E_{i+\frac{1}{2}}} \qquad r^{R}_{i+\frac{1}{2}} = \frac{\delta E_{i+\frac{3}{2}}}{\delta E_{i+\frac{1}{2}}} \tag{7}$$

The different flux limiters are displayed in figure 1 graphically. These limiters are constructed based on the the TVD region bounded by the SUPERBEE and MINBEE limiters. The SUPERBEE limiter is the least diffusive limiter possible and may induce small oscillations around strong gradients. MINBEE is the most diffusive limiter. In this study the MC-limiter [6] is used for all simulations.

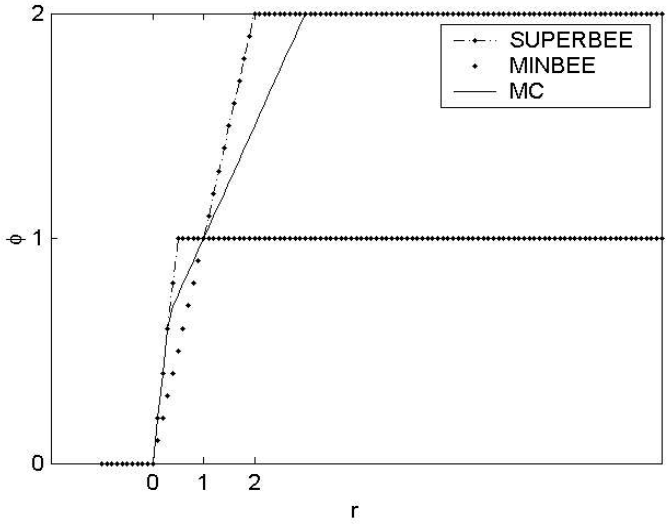

Figure 1. Flux limiters as functions of r

The flux limiter for the inter cell boundary i+1/2 is chosen as the smallest limiter value of the left and right slopes.

$$\phi_{i+\frac{1}{2}} = min(\phi(r^{L}_{i+\frac{1}{2}}), \phi(r^{R}_{i+\frac{1}{2}})) \tag{8}$$

The FLIC scheme is then written as

$$\boldsymbol{F}^{\boldsymbol{FLIC}}_{\boldsymbol{i+\frac{1}{2}}} = \boldsymbol{F}^{\boldsymbol{FORCE}}_{\boldsymbol{i+\frac{1}{2}}} + \phi_{i+\frac{1}{2}}\left[\boldsymbol{F}^{\boldsymbol{RI}}_{\boldsymbol{i+\frac{1}{2}}} - \boldsymbol{F}^{\boldsymbol{FORCE}}_{\boldsymbol{i+\frac{1}{2}}}\right] \tag{9}$$

The diffusion terms are solved by time splitting. First the Euler equations are solved by the TVD scheme, then a set of parabolic PDEs, as equation 10, are solved with the initial condition given by the solutions of the Euler equations.

$$\frac{\partial \boldsymbol{U}}{\partial t} = \frac{\partial}{\partial x}\left(\Gamma \frac{\partial \boldsymbol{H}}{\partial x}\right) \tag{10}$$

2.2 Turbulence Model

To model the sub-grid scale turbulence, the code uses a model proposed by Menon et. al. [2]. The model is a conservation equation of the turbulent kinetic energy, k, with a production term and a destruction term, as shown in equations 12-16.

$$\frac{\partial \bar{\rho} k}{\partial t} + \nabla \cdot \left(\bar{\rho} \tilde{\boldsymbol{u}} k \right) = \nabla \cdot \left(\bar{\rho} \frac{\nu_t}{\sigma_t} \nabla k \right) + P^{sgs} - D^{sgs} \tag{11}$$

$$P^{sgs} = -\tau_{ij} \frac{\partial \tilde{u}_i}{\partial x_j} \tag{12}$$

$$\tau_{ij} = -2\ \bar{\rho} \nu_t \left(S_{ij} - \frac{1}{3} S_{kk} \delta_{ij} \right) + \frac{2}{3} \bar{\rho} k \tag{13}$$

$$\nu_t = C_s k^{\frac{1}{2}} \Delta \tag{14}$$

$$D^{sgs} = \frac{C_\epsilon \bar{\rho} k^{\frac{3}{2}}}{\Delta} \tag{15}$$

2.3 Combustion model

The code uses two different methods of solving the chemical reaction terms of the energy equation shown in equation 16. The first method is used if the reaction wave is a laminar or turbulent combustion wave. This method is a Riemann solver based on the solver presented by Teng et. al. [7] that assumes an infinitely thin flame. The reaction variable z is either 0 or 1 depending whether the state is burnt or unburned. The burning velocity is modelled by a model, presented by Flohr and Pitsch [8], for industrial burners.

$$\frac{\partial G}{\partial t} + v_f \nabla G = S_T |\nabla G| \tag{16}$$

To track the flame, the G-equation for turbulent flames [3], is used, eq. 16. It assumes that the variable G is a smooth function which is positive in burned gas and negative in the unburned gas. The flame front is set as G equals zero. By placing the flame front as a set value of a smooth function the discontinuous nature of the infinitely thin flame can be handled.

$$\frac{\partial \left(\tilde{E} + \bar{\rho} q \tilde{z} \right)}{\partial t} + \nabla \cdot \left(\tilde{\boldsymbol{u}} \left(\tilde{E} + \bar{\rho} q \tilde{z} + \tilde{p} \right) \right) = 0 \tag{17}$$

A second reaction variable, α, which describes the concentration of radicals, is solved as a conserved variable, shown in equation 18. The reaction source term is an Arrhenius function. In the burnt state α is 1 and initially α is 0 in the unburned gas. If the value of α reaches 1 in the unburned gas, the mixture ignites and a second model for the rate of z is used.

$$\frac{\partial \bar{\rho} \alpha}{\partial t} + \nabla \cdot \left(\bar{\rho} \tilde{\boldsymbol{u}} \alpha \right) = \boldsymbol{r}_\alpha \tag{18}$$

Equation 18 is solved with the assumption that all released energy from the reaction is used to increase the pressure and that the velocity and density is constant. Equation 19 describes the rate of change of z due to the chemical reactions. The reaction rate model was presented by Korobeinikov et.al. [9].

$$\frac{dz}{dt} = -k_2\, p^{n_2} \rho^{l_2} z^{m_1} \exp\left(\frac{-E_2}{RT}\right) + k_3\, p^{n_3} \rho^{l_3} (1-z)^{m_2} \exp\left(\frac{-(E_2+Q)}{RT}\right) \tag{19}$$

For the experiments with stoichiometric hydrogen-air in this paper the constants in equation 19 are set as

$l_2=l_3=0$, $n_2=n_3=2$, $m_1=m_2=2$, $k_2=k_3=3.9\cdot10^{-7}$, $E_2=2000$ J/kg, $Q=3.6\cdot10^6$ J/kg

3.0 EXPERIMENTS

The numerical experiment is as similar to the physical experiment as possible. The temperature and pressure of both experiments are assumed to be 20°C and 1 atm. In chapters 3.1 and 3.2 the set-up of both types of experiments are explained.

3.1 Experimental setup

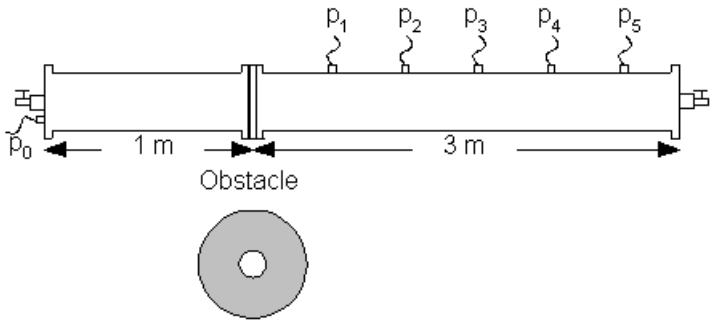

Figure 2. Experimental tube and pressure transducer configuration

The experiment is performed in a 4 m long circular steel tube with inner diameter of 0.107 m. The pipe is closed in both ends and has a spark ignition source in one end. An obstacle with circular opening is fitted 1 m from the ignition source, see figure 2. The opening of the obstacle is 30 mm, which is a blockage ratio of 0.92. This obstacle causes DDT in experiments with stoichiometric hydrogen. The hydrogen-air mixture is filled into the tube at the ignition end at 1 atm and at room temperature. To measure the pressure, six transducers are mounted on the tube. Transducer P0 is mounted at the ignition point. The other transducers are mounted at 0.5 m intervals behind the obstruction, starting at 0.5 m from the obstacle. P0, P1 and P3 are Kistler 7001 type transducers and P2, P4 and P5 are Kistler 603B transducers. Figure 3 show the pressure records of the experiment described. The speed of the detonation wave is approximately 2000 m/s. P0 show a slow increase in the pressure in the ignition end of the tube. The obstacle creates turbulence and reflected waves which influence the flame propagation and reaction rate. The obstacle also create a jet behind it which is supersonic when the flame passes. The DDT occurs in or at the edge of that jet. Figure 3 show the experimental pressure records of the described experiment.

3.2 Numerical setup

The geometry of the numerical setup is an approximation of the physical experiments with cylinder coordinates. This is a rough assumption, since the equations are filtered for LES, and the largest length scales of the turbulence are directly simulated. The velocity gradients are strongest in the radial and axial direction because of the geometry, so omitting the tangential direction should not influence the production of turbulence too much. The ignition is approximated by a few computational cells that are set as burnt, this will start the combustion wave. In these numerical experiments the grid resolutions are 2 mm. The number of cells are 2000 in the x-direction and 25 in radial direction. The CFL number is 0.9 for all time steps. The Smagorinsky constant is 0.17 and the constant in the turbulent destruction term in the turbulence model is 0.8. No heat transfer between the gas and the tube wall is modeled in these simulations.

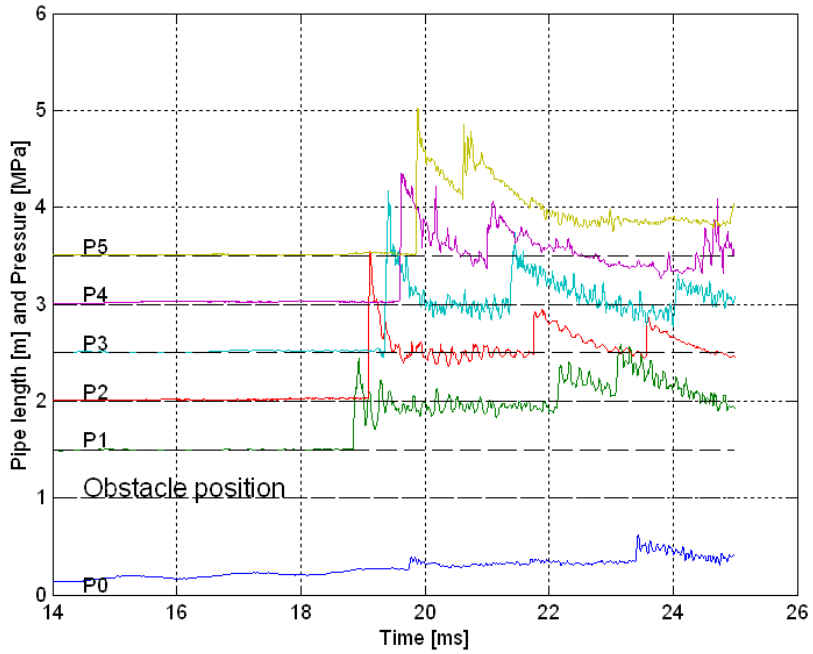

Figure 3. Pressure records from the physical experiment

4.0 RESULTS

The simulated pressure matches the pressure from the experiment at ignition end of the tube to some degree, as shown in figure 4. As the flame gets closer to the obstacle, the difference between the numerical results and the experimental results becomes more evident.

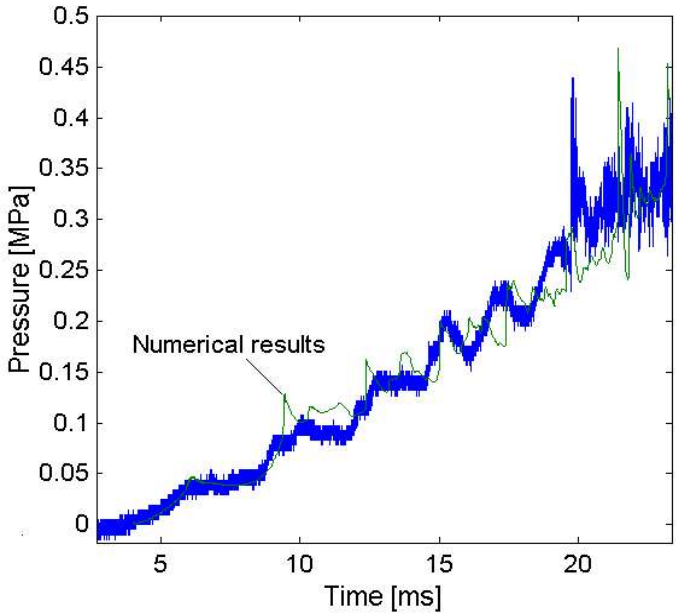

Figure 4. Pressure histories from numerical and physical experiment at transducer P0

The sharp pressure peak at around 19 ms in the physical experiment, resulting from the DDT, is simulated at a later time than in the experiment. This is because the simulated DDT occurs later than in the experiment. This discrepancy may be a result of many factors. The interaction of the flame with the obstacle may not be handled correctly. The boundary conditions for the variable G is not well defined at walls and the flame may not be propagated correctly through the obstacle. The modeled turbulence and burning velocity are also important factors that may contribute to the discrepancies. The burning velocity closure model may not be able to model the reaction rate accurately when the flame is close to the obstacle, because the flame may not be as thin as assumed. Anther likely factors that may create errors are that the grid size may be too large, so that a possibly simulated hot spot may be averaged to a too low temperature that will not produce a DDT. There may also be effects from the tangential direction. DDT may be a strictly 3D phenomena and reflected and focused shocks should then be simulated in 3D as, of course, the turbulence.

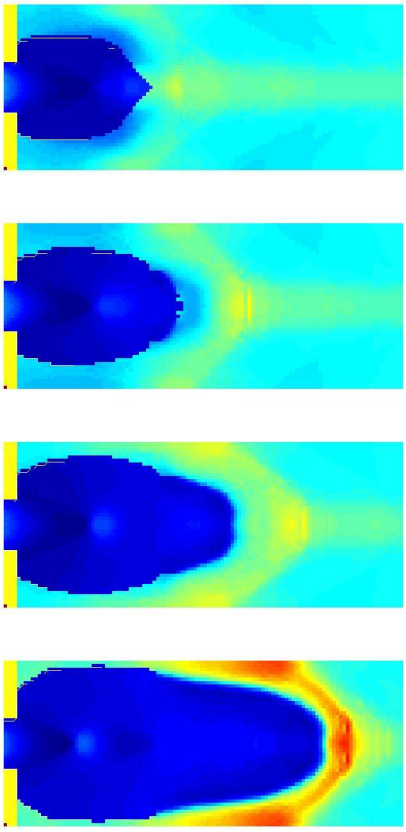

Figure 5. Density in a 240 mm x 107 mm area behind the obstacle. The time difference between images is about 0.025 ms.

Figure 5 show the simulated DDT behind the obstacle. The second image from the top show that a DDT has occurred. The density show a smooth gradient between the burned and unburned gas in the small area where the flame is a detonation front. The detonation propagates with a speed higher than the shock speed and will eventually catch up with the shock. The flow has a simulated Mach-number of about 2.2 in the jet when the flame passes the obstacle, as shown in figure 6. This creates oblique shocks and expansion waves. It seems that the DDT occurs when the flame interacts with one of these waves. Figures 7 and 8 show the pressure histories at sensor P2 and P5, where it can be seen that the pressure level and propagation speed of the detonation wave is simulated accurately. There are an offset of just over 2 ms between the simulated and the experimental detonation front both at transducer P2 and P5. This indicates that the constants in the reaction rate model used for reaction variable z is good enough to predict the reaction of a stoichiometric mixture of hydrogen-air in a detonation wave, and that the reaction rate for variable α, which calculates the induction time, is good enough as well.

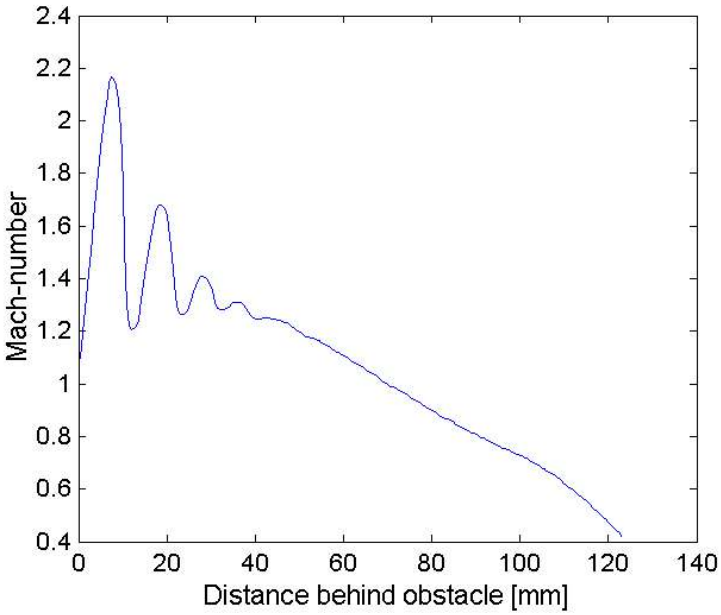

Figure 6. Simulated Mach-number behind obstacle at central axis. The flame is 20 mm in front of the obstacle.

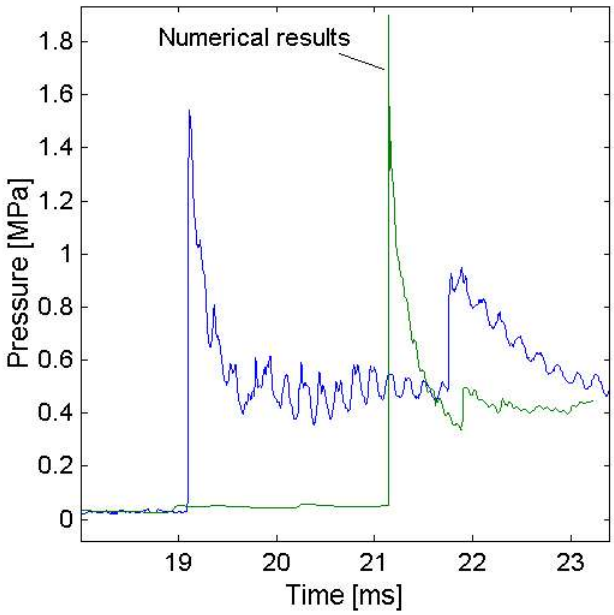

Figure 7. Pressure histories from numerical and physical experiment at transducer P2

5.0 CONCLUSION

The code is capable of simulating laminar and turbulent combustion waves, DDT and detonation waves. The simulation results are showing some errors compared with the physical experiment with this set-up. It is impossible to say if the position of the DDT is simulated correctly with these results, but it seems that the DDT is simulated too far behind the obstacle, since it occurs later than in the experiment. This may be a result of a too coarse grid or the boundary conditions in the flame propagation model. The assumption of 2D is also a probable reason for the errors in the simulation of DDT. The detonation wave is simulated nearly correctly, which indicates that the two-step model is working satisfactory with the constants presented here

for stoichiometric hydrogen-air. The most important future work with this code is to improve the implementation of the G-equation, specifically the boundary conditions at walls. This equation control the flame propagation and is very important for the simulation of the turbulent combustion waves. Adaptive mesh refinement may also produce better results, because it is then possible to use a finer mesh around the reaction front and shock fronts and a coarse mesh away from the fronts to save computing time.

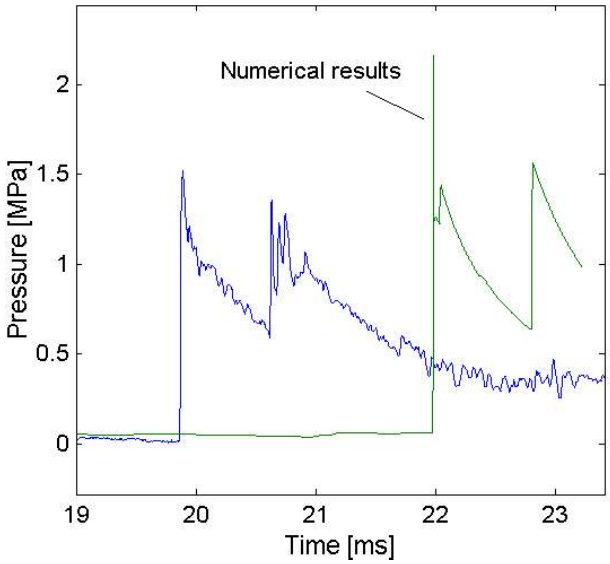

Figure 8. Pressure histories from numerical and physical experiments at transducer P5

REFERENCES

1. Toro, E.F., Riemann Solvers and Numerical Methods for Fluid Dynamics, A Practical Introduction, 1999, Springer-Verlag Berlin Heidelberg.
2. Menon, S., Sankaran, V., Stone, C., Subgrid Combustion Modelling for the Next Generation National Combustion Code, 2003, NASA Glenn Research Center NASA/CR-2003-212202.
3. Peters, N., Turbulent Combustion, 2000, Cambridge University Press, United Kingdom.
4. Vaagsaether, K., Bjerketvedt, D., Simulation of Supersonic Shear Layers with High Resolution TVD Methods, Fourth International Conference on CFD in the Oil and Gas, Metallurgical & Process Industries, 6-8 June 2005, Trondheim, Accepted.
5. Knudsen, V., Vaagsaether, K., Bjerketvedt, D., Experiments with hydrogen-air explosions in a closed pipe with a single obstacle, Proceedings of the European Combustion Meeting, 3-6 April, 2005, Louvain-la-Neuve.
6. Leveque, R., Finite Volume Methods for Hyperbolic Problems, 2002, Cambridge University Press, United Kingdom.
7. Teng, T.H., Chorin, A.J., Liu, T.P., Riemann Problems for Reacting Gas, with Applications to Transition, 1982, SIAM J. Appl. Math. Vol. 42 No. 5, pp. 964-981.
8. Flohr, P., Pitsch, H., A Turbulent Flame Speed Closure Model for LES of Industrial Burner Flows, 2000, Center for Turbulence Research, Proceedings of the Summer Program
9. Korobeinikov, V. P., Levin, V. A., Markov, V. V., Chernyi, G. G., Propagation of Blast in a Combustible Gas, 1972, Astronautica Acta. Vol. 17, pp. 529-537.